photonics

MDPI

Article

Extraordinary light trapping enhancement in silicon solar cell patterned with graded photonic super-crystals (Manuscript ID: photonics-248146)

Safaa Hassan [1], David Lowell [1], Murthada Adewole [1], David George [1], Hualiang Zhang [2], and Yuankun Lin [1,3,*]

[1] Department of Physics, University of North Texas, Denton, TX 76203, USA; SafaaHassan@my.unt.edu (S.H.); DavidLowell@my.unt.edu (D.L.); murthadaadewole@my.unt.edu (M.A.); davidgeorge2@my.unt.edu (D.G.);
[2] ECE Department, University of Massachusetts Lowell, Lowell, MA 01854, USA; hualiang_zhang@uml.edu
[3] Department of Electrical Engineering, University of North Texas, Denton, TX 76203, USA
* Correspondence: yuankun.lin@unt.edu; Tel.: +1-940-565-4548

Received: date; Accepted: date; Published: date

Abstract: For the first time, we have studied the light trapping enhancement in newly discovered graded photonic super-crystals with dual periodicity and dual basis. Broadband, wide incident angle, and polarization independent light trapping enhancement was achieved in silicon solar cells patterned with the graded photonic super-crystals. The design of the graded photonic super-crystals is flexible and efficient as they can be realized by multi-beam interference. The optical response of the patterned silicon solar cell retains the Bloch-mode resonance; however, the light absorption is greatly enhanced in broadband wavelengths due to the graded, complex unit super-cell nanostructures, leading to the overlap of Bloch-mode resonances. The broadband, wide angle light coupling and trapping enhancement mechanism are understood to be due to the spatial variance of the index of refraction due to varying filling fraction, dual-basis, and varying lattice constants in different directions.

Keywords: light trapping; photonic crystals; micro- and nano-structured materials; photovoltaic devices

---

1. Introduction

When solar cells become thinner, ultrathin materials used in the solar cells become almost transparent and have low efficiencies to trap or absorb light. Advanced light trapping techniques are required for solar cells to achieve high efficiencies. Nanostructures have been used to improve light coupling from free space to silicon based photovoltaic solar cell devices and incorporate light-trapping functionality in the solar cell in order to increase the light absorption of the device. Various nanostructures have been proposed and their mechanisms for light absorption enhancement have been investigated, which include surface plasmon induced enhancement [1], nanowire-based light trapping [2-4], back-reflector-based multiple pass absorption [5-9], and one-dimension and two-dimension photonic crystal-based structural resonances [10-14]. Photonic crystals are periodic structures that offer powerful photon control and manipulation capability [10-11]. The structural resonances in simple photonic crystals offer a series of sharp resonances at a specific wavelengths and angles [10-14]. By incorporating dual lattice or so-called superlattice structures into photonic crystals, the spectral response of the photon-lattice interactions can be broadened [15-18].

Small amounts of position disorder in photonic lattices can be used to control light coupling into the lattice by controlling the ratio of Bloch-mode resonances to Anderson-localized modes and to improve light trapping in solar cell devices [15,19,20]. Furthermore, designs using randomly or quasi-randomly textured surfaces have achieved both high efficiency light trapping through coherent light scattering and broadband, wide angle optical properties due to the introduced disorders [15,21-24]. The strong Bloch mode-based resonant absorption in narrow bandwidths and broadband absorption with enhancement can be balanced by controlling the degree of disorder in the nanostructured device; however, this can be difficult [19,21].

In this paper, for the first time, we have studied light trapping enhancement in silicon patterned with nanostructures that can be considered as a hybrid of photonic crystals and disorder. High resonance absorption and broadband optical response were simultaneously achieved in silicon patterned with graded photonic super-crystals (GPSCs) with dual basis and dual periodicity. In contrast to wavelength broadening due to disorder in the nanostructures, the broadband and wide angle optical response in the newly discovered GPSCs was achieved through gradient refractive index in dual basis nanostructures.

2. Description of Graded Photonic Super-crystals and Simulation Methods

Using the results of Oskooi et al [19] as a comparison, similar solar cell structures were used in the simulations with the GPSC pattern instead of a disordered photonic crystal pattern. As shown in Figure 1(a), a 300 nm indium-tin oxide (ITO) (n=1.8) covered glass slide can be spin-coated with a positive resist, then patterned with the newly discovered GPSC [25,26] as shown in Figure 1(b), and finally etched to a depth of 200 nm. A gold film is then deposited and the positive resist is lifted off. The gold film will initiate the silicon growth for 200 nm (fill the groove of the pattern) [27]. Gold is again deposited the whole flat surface to initiate the silicon film growth for a thickness of 300 nm. Then the gold film is etched away. A 50 nm silver film is deposited as the metal back-reflector following 100 nm ITO deposition.

The lattice constant, a, was used to describe the feature size of the nanostructure as shown in Figure 1(b) for a 12a×12a unit super-cell of GPSC. If the parameter a is less than 500 nm, electron-beam lithography can be used for the fabrication GPSC pattern. An SEM of a fabricated GPSC using electron-beam lithography in the positive resist PMMA is shown in Figure 1(c). When the lattice constant is above 500 nm, eight-beam interference lithography (four inner beams with an interference angle of α and four outer beams with an interference angle of β) can be used to fabricate the pattern [26,27]. A GPSC with a unit super-cell size of 26a×26a (with a=1100 nm) has been fabricated using eight-beam interference [27]. The unit super-cell size can be controlled by the selection of angles α and β [27]. It is easier to fabricate a GPSC with a large unit super-cell than one with a small unit super-cell. However, it is difficult to have a high resolution simulation for a GPSC with a large unit super-cell. We expect that a GPSC with a unit super-cell of 12a×12a can be achieved with experimental fabrication and high resolution simulation. The authors acknowledge that the lattice constant, a, is not in the right range; however, this paper focuses on the simulations only and the experimental results will be published in the future when the GPSC with the desired structural parameters has been fabricated and characterized.

In the simulation, the eight-beam interference patterns were converted to binary complex dielectric structures by comparing the interference intensity, I(r), with a threshold intensity, I_{th} (as a percentage of maximum intensity), using the following step functions: complex dielectric material=silicon, when $I < I_{th}$, and complex dielectric material=ITO when $I > I_{th}$. A complex dielectric function of amorphous silicon should be used. However, the complex dielectric function of amorphous silicon depends on the growth conditions [28] and no tabulated data was found. Furthermore, this paper will compare structural resonance difference between silicon patterned with a GPSC and silicon patterned with a conventional photonic crystal. The selection of optical parameters of silicon will have less effects on the resonance peaks than the structural parameters of the photonic crystals. In this paper, we have used tabulated data of the optical properties (refractive index and extinction coefficient) of crystalline silicon from 250 to 1000 nm [29]. Nano-structuring of silicon using GPSCs and conventional photonic crystals show little difference in improving light trapping in the high absorption region. Thus the simulations are presented in the wavelength range between 500 and 1000 nm. Figures 1(b) shows a permittivity structure output that is used to check the accuracy of the simulation program in MIT MEEP.

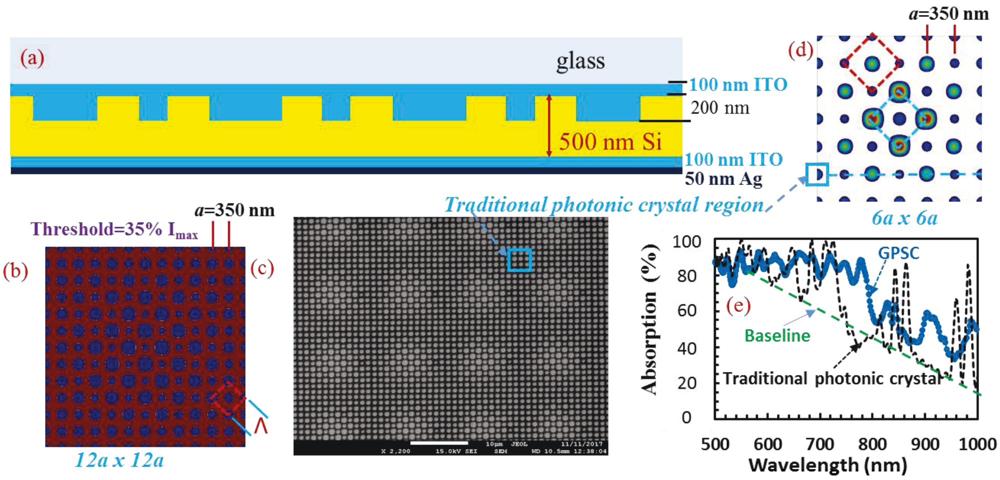

Figure 1. (a) Schematic of a silicon photovoltaic device patterned with a GPSC on a silicon (Si) absorbing layer. (b) Permittivity structures output from MIT's MEEP simulation with a unit super-cell size of 12a×12a (a=350 nm, the red region is silicon and the blue region is ITO). (c) SEM of fabricated GPSC in PMMA using e-beam lithography. (d) A unit super-cell size of 6a×6a (a=350 nm) formed by eight-beam interference with a threshold intensity I_{th}=30% of the maximum. (d) An eight-beam interference pattern with a unit super-cell of 6a×6a (a=350 nm). The dashed squares link lattices at corners that belong to one set of graded lattice. (e) Absorption spectra for silicon patterned with GPSC with a unit cell of 6a×6a, and with a traditional photonic crystal with a unit cell size of 350×350 nm^2 with silicon and a circle of ITO with 145 nm diameter in the center. The dashed green line indicates the baseline of absorption for eye guidance.

The simulations of absorption fraction in silicon patterned with the GPSC and conventional photonic crystal were performed using MIT's open-source finite-difference time-domain (FDTD) software tool [30] via the Simpetus Electromagnetic Simulation Platform in Amazon Web Services (AWS). Due to the large unit super-cell size, 36-core virtual machines in AWS were selected for parallel computations. For the unit super-cell size of 12a×12a, a resolution as large as 22 can be used corresponding to an estimated mesh size of 350/22=15.9 nm (about 1/31 of 500 nm light wavelength). For an accurate comparison of the silicon patterned with the GPSC and conventional photonic crystal, a unit super-cell size of 6a×6a as shown in Figure 1(d) and a resolution as large as 40 is used corresponding to an estimated mesh size of 350/40=8.8 nm. For the structure in Figure 1(a) with a silver layer as a reflector, the transmission T(λ) is zero. In the simulation, only the reflection R(λ) was calculated and plotted. Using A(λ)=1-T(λ)-R(λ), an absorption was obtained. An integrated absorption can be calculated using the tabulated AM 1.5G solar spectrum. However, this was not done in order to compare results with others under the same conditions [19-20]. Sunlight is almost unpolarized. To best explain the simulations, the average values of the simulations with incident light polarized in the [0,1] and [1,1] directions can be displayed, but in this study we chose to display them separately to analyze the polarization effects, which is one of distinguished features of silicon patterned with GPSC.

3. Results

Figure 1(d) shows a GSPC with unit super-cell of 6a×6a (a=350 nm) formed by eight-beam interference. The highest absorption occurs for the interference pattern with threshold intensity at 30% of maximum intensity. Figure 1(e) shows the absorption of 500 nm silicon patterned with a GPSC with the unit super-cell of 6a×6a and with I_{th}=30% of the maximum intensity. The absorption from

500 nm silicon patterned with a conventional photonic crystal is also shown in Figure 1(d) for comparison. The conventional photonic crystal is a square lattice with a uniform pattern (without gradient structure) as indicated by solid blue square in Figure 1(c). We picked up a pattern (as indicated by a solid blue square) near the edge of the GPSC and measured the diameter of the pattern in Figure 1(d). We used a unit cell size of 350×350 nm² square of silicon with a circle of ITO of 145 nm diameter in the center for the conventional photonic crystal. Comparing both spectra, (a) the absorption in silicon patterned with the conventional photonic crystal shows relatively sharp Bloch-mode resonance peaks while the absorption spectrum from the silicon with the GPSC shows smoothed Bloch-mode resonance peaks, similar to the spectra of silicon patterned in photonic crystal with 3.6% positional disorders in Figure 2 of reference 19; (b) despite the overall decreasing absorption baseline with increasing wavelength as indicated by the dashed green line in Figure 1(e) and that in reference 19 by Oskooi et al., the absorption in Figure 1(e) for silicon patterned with the GPSC is kept at a high level between 500 and 780 nm (i.e. broadband). The broadband light coupling can be understood by Eq. (1) [31]:

$$\frac{2\pi}{\lambda}n_{eff} - \frac{2\pi}{\lambda}\sin(\theta) = G \qquad (1)$$

where n_{eff} is the effective refractive index of the GPSC, λ is the wavelength in free space, and G is the reciprocal lattice vector. G can be 2π/a, 2π/Λ, 2π/(na) as defined in Figure 1(b), or others. $\Lambda=\sqrt{2}a$ is the periodicity in the 45 degree direction relative to the x or y axis and na (n is an integer number) is the length of the large unit super-cell, e.g. 6a.

The effective refractive index is defined as follows:

$$n_{eff} = f \times n_{ITO} + (1-f) \times n_{silicon} \qquad (2)$$

Where n_{ITO} is the refractive index of ITO, $n_{silicon}$ is the refractive index of silicon, and *f* is the fill fraction of ITO in the GPSC.

The GPSC consists of two sets of graded lattices. The dashed squares in Figure 1(d) link the corner lattices that belong to one set of the graded lattices. For example, the lattice dots linked by the dashed blue square in Figure 1(d) have a large circle in the center and gradually decrease their sizes in toward the edge the unit super-cell. The two sets of graded lattices have the same periodicity thus G parameter in Eq. (1) is the same. However, the fill fraction f is spatially varying. For example f=13.5% for a circle of ITO with 145 nm diameter in a 350×350 nm² square of silicon at the left side of the dashed blue line, while f=8.9% for a 350×350 nm² square region in the middle of the line. Due to the availability of different fill fractions, light wavelengths in a broad range can meet the condition in Eq. (1). Thus, broadband light trapping enhancement is observed in the simulation for silicon with the GPSC due to the overlap of Bloch-mode resonances.

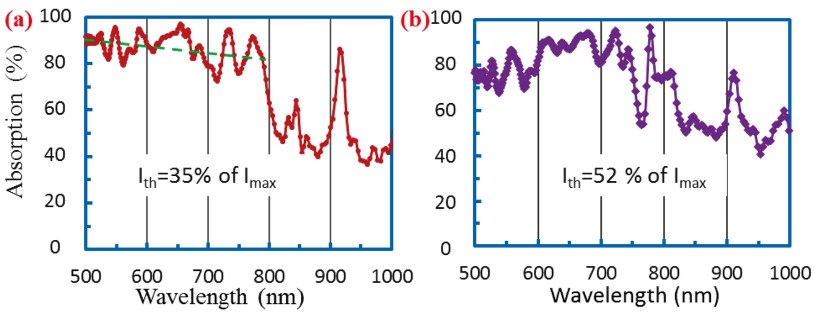

Figure 2. (a) Absorption versus wavelength profile at normal incidence for the silicon patterned with two GPSCs with unit super-cell size of 12a×12a: a GPSC of threshold intensity Ith=35% (a) and a GPSC of threshold intensity Ith=52% (b).

The degree of variation in the graded lattices depends on the location of the interference pattern as described later in the discussion section, and also on the size of unit super-cell. For GPSCs with a unit super-cell size of 12a×12a, the corner areas in Figure 1(b) and regions indicated by the solid blue square in Figure 1(c) have a uniform instead of graded lattice and become a conventional photonic crystal. The effect of the conventional photonic crystal can be seen in the absorption spectrum. For silicon patterned with a GPSC with unit super-cell of 12a×12a, a maximum average absorption occurs with I_{th}=35% of the maximum intensity, as shown in Figure 2(a). Broadband absorption and smoothed Bloch-mode resonance peaks still appear due to the graded regions of the pattern; however, the overall absorption decreases with increasing wavelength, as indicated by the dashed green line, due to the conventional photonic crystal regions. When the threshold intensity is increased from 35% in Figure 2(a) to 52% in Figure 2(b), fill fraction f is decreased and n_{eff} is increased. Therefore, the wavelength for the overall absorption maximum is also red-shifted, from Eq. (1) and (2) and as shown in the figures.

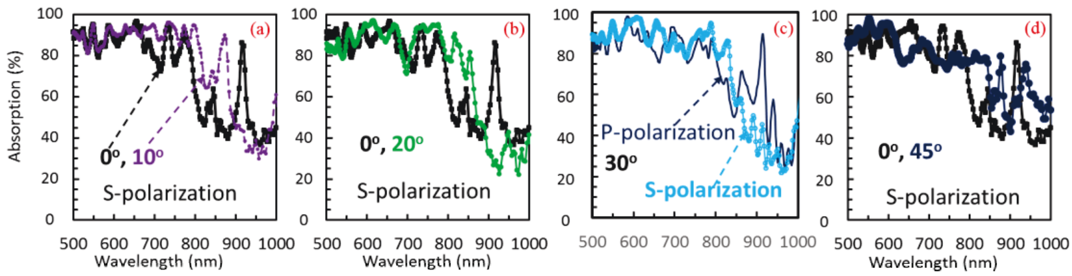

Figure 3. (a-d) Absorption spectra versus wavelength for 500 nm silicon patterned with GPSC with a unit super-cell of 12a×12a (a=350 nm) and with a threshold intensity of 35% of maximum with [1,0] polarized light at normal incidence, compared with the absorption spectrum at four off-normal angles of incidence (zenith angle=10, 20,30 and 45 degrees respectively) with s-polarization. The absorption from the silicon patterned with the GPSC at an incident angle of 30 degrees with p-polarization is also shown in (c).

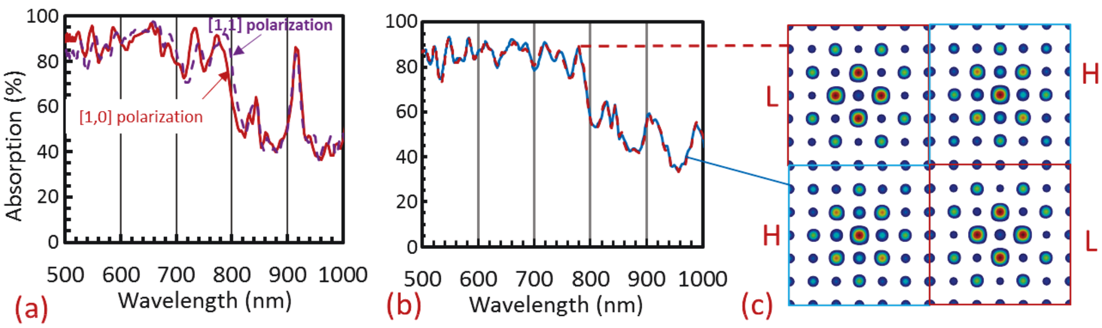

Figure 4. (a) Absorption spectra of light with polarizations in the [1,0] and [1,1] direction incident on silicon patterned with a GPSC with a unit super-cell of 12a×12a (a=350 nm), formed with a threshold of 35% of maximum interference intensity. (b) Absorption spectra of light with polarizations in the [1,0] direction incident on silicon patterned with a GPSC with a unit super-cell of 6a×6a (a=350 nm), formed with a threshold of 30% of maximum intensity for the pattern from the L and H regions in (c). (c) Eight-beam interference pattern with unit super-cell size 6a×6a, showing two distinct regions marked with an L (L for low intensity spot in the center) and an H (H for high intensity spot in the center).

Figure 3 shows the dependence on incident angle for 500 nm silicon patterned with a GPSC with a unit super-cell size of 12a×12a (a=350 nm) and a threshold intensity of 35% of the maximum intensity, for s-polarized light, or [1,0] polarization, with zenith angle of 10, 20, 30 and 45 degrees for Figure 3(a,b,c,d) respectively, and azimuth angle of 90 degrees relative to x-axis for all. Compared with the absorption spectrum at normal incidence (θ=0°), the spectrum with the incident angle of θ=10° shows higher absorption around 700 nm, high broadband absorption region expanded to 800 nm, and blue-shift of the Bloch-mode resonance peak around 900 nm. The absorption spectra at 20 and 30 degrees show almost the same light absorption as the one at 0 degrees except a broader high absorption region expanded to 800 nm. At an incident angle of 45 degrees, the simulated absorption decreases above 600 nm. Thus, under the wide angle range of 30 degrees, the absorption is almost same. For p-polarization at a zenith angle of 30 degrees in Figure 3(c), the absorption peak around 900 nm still appears and the high absorption band is a little bit narrower than that with s-polarization.

Figure 4 shows the absorption of light with polarizations in the [1,0] and [1,1] directions incident on silicon patterned with the GPSC with a unit super-cell size of 12a×12a, formed with the same threshold of 35% of maximum intensity. We can see from Figure 4 that the absorption spectra are the same when the light is incident with different polarizations. In the [1,1] direction of the GPSC, the lattice periodicity is larger, compared with that of the [1,0] direction. The gradient filling fraction in the [1,1] direction helps couple the light into the patterned structures, with similarly high enhancement as with [1,0] polarized light, by meeting the conditions in Eq. (1) and (2). Thus, we have achieved polarization-independent broadband absorption when the silicon solar cell is patterned with the GPSC.

If the GPSC is formed by eight-beam interference as shown in Figure 4(c), there are two "L" square regions where the central spot has a "low" intensity and two "H" regions where the central spot has a "high" intensity. If the unit super-cell is large, the "high" or "low" spot in the center is not critical as there are many lattice spots. However, the "high" or "low" spot in the center might become crucial in the absorption when the number of lattice spots become small. We simulated the absorption spectra for silicon patterned with GPSC with a unit super-cell size of 6a×6a with formed with a threshold of 30% of maximum intensity, as shown in Figure 4(b). The absorption from "H" region (dashed red line) is almost identical to that from "L" region (blue line).

4. Discussion

For photovoltaic devices, nanostructuring the active layers has generated high local density of optical states in the absorber layer, allowing for more energy to be coupled into the solar cell and absorbed [10-14]. The appearance of many photonic bands, up to 144, below the photonic band gap or cavity mode [25] indicates a large density of optical states in the GPSC. When light is coupled into the structure, we expect resonance modes in the GPSC, waveguide modes in the horizontal plane in the silicon and ITO regions without GPSC, and leaky resonance modes in the vertical direction. In the simulations, light source detectors were placed everywhere in a region above the top-layer ITO. These detectors can collect signals in a large angle of up to 90 degrees, but it cannot collect the waveguide modes mentioned above. In our simulations of the light extraction in organic light emitting diode devices [32], the fraction of light power in the waveguide modes is also zero. We have assumed zero reflection from waveguide modes in this study.

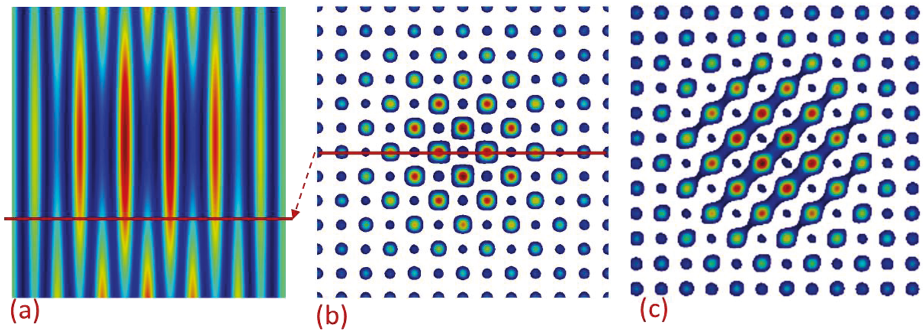

Figure 5. (a) Cross-section in the x-z plane of the eight-beam interference pattern. (b) Cross-section in x-y plane of the eight-beam interference patterned as viewed at the location indicated by the red line in (a). The pattern becomes the one in (c) when the phases of four outer interference beams are set to be (0, 0.15π, 0, 0.15π).

High resonance absorption and broadband optical response can be further studied via the optimization of iso-intensity surfaces of the interference pattern, lattice constant, and unit super-cell size. Figure 5(a) shows a cross-section in x-z plane of the interference pattern. When the sample is exposed at the location as indicated by the red line, the pattern will look like the one in Figure 5(b) where the one set of lattice spots is smaller than the other. If the red line is shifted to the bottom of Figure 5(a), the formed pattern will have a similar spot size in both sets of lattices. If the phases of the four outer interference beams were set to be (0, 0.15π, 0, 0.15π), the pattern in Figure 5(b) will become the one in (c).

5. Conclusions

For the first time, we have simulated the fraction of absorption of light in silicon solar cells where the silicon is patterned with GPSCs, which are a hybrid of photonic crystals and disorder. Due to the spatially gradient fill fraction of dielectrics and large number of available lattice constants in different directions, we have achieved broadband, wide angle, and polarization-independent absorption spectra. Broadband light trapping enhancement has been explained in terms of overlapping Bloch-mode resonances.

Acknowledgments: This work is supported by research grants from the U.S. National Science Foundation under Grant Nos. CMMI- 1661842, 1661749, and ECCS-1407443.

Author Contributions: Y.L., S.H. and H.Z. conceived and designed simulations; S.H., D.L., M.A. and D.G. performed the simulations; Y.L., S.H. and D.L. analyzed the data; D.L. contributed parallel computation tools; Y.L. and S.H. wrote the paper. All authors read and commented on the manuscript.

Conflicts of Interest: The authors declare no conflict of interest. The founding sponsors had no role in the design of the study; in the collection, analyses, or interpretation of data; in the writing of the manuscript, and in the decision to publish the results.

References

1. Atwater, H.; Polman, A. Plasmonics for improved photovoltaic devices. *Nat. Mater*. **2010**, 9, 205–513.
2. Garnett, E.; Yang, P. Light trapping in silicon nanowire solar cells. *Nano Lett*. **2010**, 10, 1082–1087.
3. Kelzenberg, M. D.; et al. Enhanced absorption and carrier collection in Si wire arrays for photovoltaic applications. *Nat. Mater*. **2010**, 9, 239.
4. Brongersma, M. L.; Cui, Y.; Fan, S. Light management for photovoltaics using high-index nanostructures. *Nat. Mater*. **2014**, 13, 451.
5. Bermel, P.; Luo, C.; Zeng, L.; Kimerling, L.; Joannopoulos, J. Improving thin-film crystalline silicon solar cell efficiencies with photonic crystals. *Opt. Express*. **2007**, 15, 16986–17000.
6. Hsu, C. M.; Battaglia, C.; Pahud, C.; Ruan, Z.; Haug, F. J.; Fan, S.; Ballif, C.; Cui, Y. High-efficiency amorphous silicon solar cell on a periodic nanocone back reflector. *Adv. Ene. Mater*. **2012**, 2, 628–633.
7. Sai, H.; Fujiwara, H.; Kondo, M.; Kanamori, Y. Enhancement of light trapping in thin-film hydrogenated microcrystalline Si solar cells using back reflectors with self-ordered dimple pattern. *Appl. Phys. Lett*. **2008**, 143501.
8. Sai, H.; Saito, K.; Kondo, M. Enhanced photocurrent and conversion efficiency in thin-film microcrystalline silicon solar cells using periodically textured back reflectors with hexagonal dimple arrays. *Appl. Phys. Lett*. **2012**, 173901.
9. Chutinan, A.; Kherani, N. P.; Zukotynski, S. High-efficiency photonic crystal solar cell architecture. *Opt. Express*. **2009**, 17, 8871-8878.
10. Mallick, S.; Agrawal, M.; Peumans, P. Optimal light trapping in ultra-thin photonic crystal crystalline silicon solar cells. *Opt. Express*. **2010**, 18, 5691–5706.
11. Bozzola, A.; Liscidini, M.; Andreani, L. C. Photonic light-trapping versus Lambertian limits in thin film silicon solar cells with 1D and 2D periodic patterns. *Opt. Express*. **2012**, 20, A224.
12. Han, S.; Chen, G. Toward the lambertian limit of light trapping in thin nanostructured silicon solar cells. *Nano Lett*. **2010**, 10, 4692–4696.
13. Sheng, X.; Liu, J.; Kozinsky, I.; Agrawal, A.; Michel, J.; Kimerling, L. Design and non-lithographic fabrication of light trapping structures for thin film silicon solar cells. *Adv. Mater*. **2011**, 23, 843–847.
14. Park, Y.; Drouard, E.; El Daif, O.; Letartre, X.; Viktorovitch, P.; Fave, A.; Kaminski, A.; Lemiti, M.; Seassal, C. Absorption enhancement using photonic crystals for silicon thin film solar cells *Opt. Express*. **2009**, 17, 14312-14321.
15. Callahan, D. M.; Horowitz, K. A.; Atwater, H. A. Light trapping in ultrathin silicon photonic crystal superlattices with randomly-textured dielectric incouplers. *Opt. Express*. **2013**, 21, 30315-30326.

16. Rinnerbauer, V.; et al. Superlattice photonic crystal as broadband solar absorber for high temperature operation. *Opt. Express*. **2014**, 22, A1895.
17. Rinnerbauer, V.; et al. Nanoimprinted superlattice metallic photonic crystal as ultraselective solar absorber. *Optica*. **2015**, 2, 743.
18. Hendrickson, J.; et al. Wideband perfect light absorber at midwave infrared using multiplexed metal structures. *Opt. Lett*. **2012**, 37, 371.
19. Oskooi, A.; Favuzzi, P.; Tanaka, Y.; Shigeta, H.; Kawakami, Y.; Noda, S. Partially-disordered photonic-crystal thin films for enhanced and robust photovoltaics. *Appl. Phys. Lett*. **2012**, 100, 181110.
20. Oskooi, A.; De Zoysa, M.; Ishizaki, K.; Noda, S. Experimental Demonstrtion of Quasi-resonant Absorption in Silicon Thin Films for Enhanced Solar Light Trapping. *ACS Photonics*. **2014**, 1, 304–309.
21. Martins, E.; Li, J.; Liu, Y.; Depauw, V.; Chen, Z.; Zhou, J.; Krauss, T. Deterministic quasi-random nanostructures for photon control. *Nat. Commun*. **2013**, 4, 2665.
22. Vynck, K.; et al. Photon management in two-dimensional disordered media. *Nat. Mater*. **2012**, 11, 1017.
23. Rockstuhl, C.; et al. Comparison and optimization of randomly textured surfaces in thin-film solar cells. *Optics Express*. **2010**, 18, A335.
24. Ferry, V. E.; et al. Optimized Spatial Correlations for Broadband Light Trapping Nanopatterns in High Efficiency Ultrathin Film a-Si:H Solar Cells. *Nano Letters*. **2011**, 11, 4239.
25. Lowell, D.; Lutkenhaus, J.; George, D.; Philipose, U.; Chen, B.; Lin, Y. Simultaneous direct holographic fabrication of photonic cavity and graded photonic lattice with dual periodicity, dual basis, and dual symmetry. *Opt. Express*. **2017**, 25, 14444.
26. Nukala, P.; Sapkota, G.; Gali, P. and Philipose, U. Transport properties of Sb doped Si nanowires. *Journal of Crystal Growth* **2012**, 353, 140.
27. Lowell, D.; Hassan, S.; Adewole, M.; Philipose, U.; Chen, B.; Lin, Y. Holographic fabrication of graded photonic super-crystals using an integrated spatial light modulator and reflective optical element laser projection system. *Appl. Opt.* (in press).
28. Janai, M.; Allred D.; D.C.Booth. D.; and Seraphin, B. Optical properties and structure of amorphous silicon films prepared by CVD. *Solar Energy Materials* **1979**, 1,11-27.
29. Green, M. Self-consistent optical parameters of intrinsic silicon at 300 K including temperature coefficients. *Solar Energy Materials & Solar Cells* **2008**, 92, 1305– 1310.
30. Oskooi, A.F.; Roundy, D.; Ibanescu, M.; Bermel, P.; Joannopoulos, J.D.; Johnson, S. MEEP: A flexible free software package for electromagnetic simulations by the FDTD method. *Compu. Phys. Commun*. **2010**, 181, 687–702.
31. Shi, J.; Pollard, M. E.; Angeles, C. A.; Chen, R.; Gates, J.C. M. D. B. Charlton Photonic crystal and quasi-crystals providing simultaneous light coupling and beam splitting within a low refractive-index slab waveguide. *Scientific Reports*. **2017**, 7, 1812.
32. Hassan, S.; Lowell, D.; Yuankun, L. High light extraction efficiency in organic light-emitting diodes by patterning the cathode in graded superlattice with dual periodicity and dual basis. *J. Appl. Phys*. **2017**, 121, 233104.